RESEARCH   **Open Access**

Average effective subcarrier-domain sparse representation approach for target information estimation in CP-OFDM-based passive bistatic radar

Zhixin Zhao[1*†], Yanghang Gong[1†], Huilin Zhou[1†] and Yulong Cao[1†]

[†]Zhixin Zhao, Yanghang Gong, Huilin Zhou and Yulong Cao contributed equally to this work.

*Correspondence:
zhaozhixin@ncu.edu.cn

[1] Information Engineering School, Nanchang University, Nanchang 330000, Jiangxi, China

Abstract

Although some existing sparse representation (SR) methods are robust for target detection in passive bistatic radar (PBR), they still face the challenges of high computational complexity and poor detection performance for extremely low-signal-to-clutter ratio (SCR) target. So, an average effective subcarrier (AES)-domain sparse representation approach is investigated in this paper. Firstly, the AES-based SR model is proposed to solve the problem of high computational complexity, which is established by utilizing the sparseness of the orthogonal frequency-division multiplexing (OFDM) with cyclic prefix (CP) signals in each effective subcarrier domain. Then, considering the difficulty of detecting extremely low-SCR targets, clutter cancellation is implemented by the SR-based optimization model. Two AES-S algorithms, namely AES-S-based clutter cancellation in the time domain (AES-S-T) and AES-S-based clutter cancellation in the subcarrier domain (AES-S-C), are proposed, and the computational complexity is further reduced. Finally, extensive simulation and experimental results illustrate that the proposed algorithms have good detection performance and low computational complexity in PBR detection scene.

Keywords: Passive bistatic radar, Sparse representation, Effective subcarrier, Low signal-to-clutter ratio

1 Introduction

Passive bistatic radars (PBRs) do not emit electromagnetic waves, but use a variety of communication and broadcasting signals as illuminators of opportunity, to passively receive the reflected echo signals from target for target detection. Nowadays, many digital communication signals, such as Digital Audio Broadcasting (DAB) [1], Digital Video Broadcasting on Terrestrial (DVB-T) [2], Digital Radio Mondiale (DRM) [3], China Digital Radio (CDR) [4], Wi-Fi [5] and Global System for Mobile Communications (GSM) [6], are modulated by orthogonal frequency-division multiplex (OFDM) modulation with cyclic prefix (CP-OFDM). The continuous radiation and omnidirectional low-altitude coverage of these signals make them easy to detect low-altitude targets. Thus, these

advantages make CP-OFDM-based PBR become a research hotspot. In CP-OFDM-based PBR, the target information is commonly estimated from the range-Doppler (RD) map obtained by the cross-ambiguity function (CAF) of surveillance and reference channel signals. However, because of the complexity of propagation environment, the unwanted direct-path signal and multipath echoes (referred to as clutter) in PBR can lead to masking of targets [7]. Thus, clutter suppression techniques become the basic steps of target detection and parameter estimation in PBR signal processing.

So far, clutter suppression techniques, including [8–11], mainly focus on the spatial domain and time domain. In spatial domain, they suppress clutter by steering nulls at the clutter directions. In time domain, the classical approaches remove clutter basing on the theory of adaptive coherent subtraction. Furthermore, another time-domain approach is extensive cancellation algorithm (ECA) and its variants (ECA-B [12], ECA-S [13], ECA-C [14]) that utilize reference signal to construct a clutter subspace matrix and achieve clutter suppression by eliminating the projected components of surveillance signal in the clutter space. All of these techniques can be used to effectively eliminate clutter at low Doppler frequencies, but they will also result in omitting targets with low Doppler frequency. Moreover, the sidelobes produced by strong targets will introduce false values into their adjacent Doppler cells, resulting in incorrect position and amplitude estimations of weak targets [15].

In recent years, sparse representation (SR) theory has been widely studied and has provided a new idea for radar signal processing [16]. Signal processing methods based on SR have been proposed in the context of radar for various applications, such as ground-penetrating radar [17], synthetic aperture radar [18], through-wall radar imaging [19] and inverse synthetic aperture radar [20]. The applications of combining SR with the sparsity of PBR scenes have also appeared in PBR signal processing. In [21], using the sparsity of received signals in the time domain as a constraint, the authors studied the target detection method based on the SR model of time-domain signal data and improved the iterative calculation steps to accelerate the computational speed. However, the long computation time prevents its implementation for real-time applications, especially when high sampling rate and long integration time are desired. In [22], a high-resolution real-time target detection sparse model of RD-domain data for PBR was built. The model was combined with the classical batch algorithm to split the long-received signal into multiple short batches. Then, based on the Doppler frequency approximation, a one-dimensional (1-D) cross-correlation is performed on each batch using fast Fourier Transform to generate the sparse model. In [23], allowing for the fact that the number of effective subcarriers (ESs) in CP-OFDM signals is far less than the total number of subcarriers, the authors proposed an ES-based SR method to realize target detection of PBR. Although the sparse methods in these papers have good target detection performance, they still face the problem of high dimensionality of sparse dictionary. Therefore, how to reduce the high computation caused by the high dimensionality of sparse dictionary of PBR target detection based on SR still needs further study. In addition, if there are low-signal-to-clutter (SCR) targets in the surveillance signal that are much weaker than the power of the clutter, then the dictionary of the existing SR methods need to be set large enough to detect these targets, which will further increase the

computational load, and even if the dictionary is set large enough, the existing SR methods may not be able to accurately detect the target.

As shown in [23], when the signal of PBR is modulated by CP-OFDM, the data carried by the received signal in the ES domain is sparse. So, using the sparse structure of the signal itself is a way to speed up the calculation of algorithm. In this paper, we propose the average ES (AES)-domain SR model for target detection and parameter estimation based on this characteristic. Different from [23] which transformed the data carried by all ESs into 1-D data to establish the SR model, the AES-based SR model proposed in this paper is a process of adding and dividing the data carried by each ES of the signal. Compared with existing SR models, the AES-based SR model significantly reduces the dictionary dimension, bringing significant computational advantages. In addition, in order to further reduce the high computational load and detect weak targets with lower-SCR, we innovatively propose a stepwise estimation method based on AES (AES-S) to realize target detection in this paper. The method transforms the clutter elimination problem into an AES-based SR optimization model. Specifically, we first use the AES model to estimate the clutter coefficient, then use the estimated clutter parameters to eliminate the clutter from the received signal and finally obtain the target information by CAF between the clutter-free surveillance and reference channel signals. Compared with the AES-domain SR model, the AES-S algorithm can not only detect weak targets with lower-SCR since the integration gain for weak targets during the process of CAF, but also further reduce the computational complexity since only clutter parameters are estimated during solving the SR optimization model.

For the solving of classical SR problem, different types of algorithms have been widely studied and applied, including greedy algorithm [24], convex optimization algorithm [25] and sparse Bayesian learning algorithm [26]. The greedy pursuit algorithm has attracted much attention due to its simple structure and small computational complexity, and the orthogonal matching pursuit (OMP) algorithm [27, 28] is the mainstream approach. So, OMP is used to solve the proposed SR model for computational efficiency in this paper. Besides, in order to deal with the complex-valued radar, we extend the OMP algorithm to the complex domain, namely complex OMP (COMP) algorithm. Combining with the aforementioned AES-based SR model, we develop an AES-based COMP (AES-COMP) algorithm. Finally, we further quantitatively evaluate the proposed algorithms in terms of peak-to-sidelobe level ratio (PSLR), integrated sidelobe level ratio (ISLR), relative error (Err) and computational complexity.

The rest of the paper is organized as follows. Section 2 introduces the sparsity of PBR signal in time domain and subcarrier domain. In Sect. 3, the proposed AES-based SR model is explained in detail and the AES-COMP algorithm is introduced. In addition, to detect the lower-SCR target and further reduce the computational complexity, we propose AES-based stepwise algorithms as a remedy. Section 4 presents and assesses the simulation results. The experimental results are given in Sect. 5. We finally draw conclusions in Sect. 6.

2 Signal model

The SR model proposed in this paper takes advantage of the sparsity of the received signal of PBR in the time domain and the characteristics of signal waveform in the subcarrier domain. Thus, the time-domain signal model of PBR is given firstly in this

section. Then, combining with the CP-OFDM characteristic of opportunity illuminators, the subcarrier-domain signal model is introduced.

2.1 Time-domain signal model

As shown in Fig. 1, a typical PBR system consists of two receiving antennas. The first is known as the reference channel, and it receives signal by an antenna directly oriented to opportunity illuminators. To obtain the purified reference signal, we can extract the direct-path wave as reference signal by reconstruction methods without any multipath distributions thanks to the digital modulation of the opportunity illuminators [29]. The cleaned reference signal is given by the following:

$$x_{\text{ref}} = d(t), \tag{1}$$

where $d(t)$ is the complex envelope of direct-path wave signal. The second channel is known as the surveillance channel, which uses a directive antenna steered towards the surveillance area and collects low-power signals reflected from targets. The surveillance signal can be regarded as the transmitted signal after time delay and Doppler shift, which can be modelled as:

$$y_{\text{surv}} = \sum_{i=0}^{N_c} a_i^{\text{clu}} d\left(t - \tau_i^{\text{clu}}\right) + \sum_{q=1}^{N_q} b_q^{\text{tar}} d\left(t - \tau_q^{\text{tar}}\right) e^{j2\pi f_q t} + v(t), \tag{2}$$

where N_q and $N_c + 1$ are the number of targets and ground scatterers, respectively. a_i^{clu} and τ_i^{clu} are the complex amplitude and time delay of the ith stationary scattering component, respectively. b_q^{tar}, τ_q^{tar} and f_q are the complex amplitude, the delay and the Doppler frequency shift of the qth target, respectively. $v(t)$ is the white Gaussian noise in the surveillance channel.

By observing (2), it can be found that the echo signal can be represented as a linear combination of delay-Doppler-shifted replicas of the direct-path signal, which is the basis of SR for PBR. According to (2), the dimension of sparse dictionary in the time-domain sparse model is related to the number of delay-Doppler grids and the number of total temporal samples.
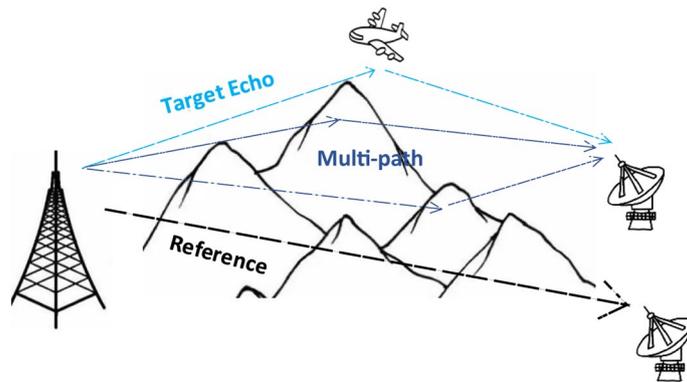

Fig. 1 Diagram of a typical PBR

2.2 Subcarrier-domain signal model

A time-domain SR model has been established in [21]. However, such a direct SR formulation will inevitably lead to large memory and computing requirements. In fact, when the opportunity illuminator of PBR is modulated by CP-OFDM, the subcarrier-domain SR models can also be established by converting the received signal to the subcarrier domain to reduce the dimensionality of sparse dictionary, which will be introduced specifically as follows. For CP-OFDM-based transmitted signal,

$$d(t) = \sum_{l=0}^{L-1} d_l(t - lT_e), \tag{3}$$

where l is the temporally consecutive index of CP-OFDM symbol. The full symbol duration is denoted as $T_e = T_g + T_s$ where T_g and T_s are the CP duration and the useful part duration, respectively. Supposing T_0 is the time-domain sampling interval, the sampling number of a whole CP-OFDM symbol is denoted as $N_e = T_e/T_0 = N_g + N_s$ where N_g and N_s are the sample sizes of a cyclic prefix and the number of subcarriers, respectively. The parameters L denotes for the number of OFDM symbols, and $d_l(t)$ denotes the lth symbol with

$$d_l(t) = \sum_{k=0}^{N_s-1} C_{l,k} e^{j2\pi k \Delta f t}, \quad -T_g < t < T_s \tag{4}$$

where k indicates the subcarrier index and $C_{l,k}$ is the normalized value of the complex modulation symbol corresponding to the lth symbol of subcarrier k. The frequency $\Delta f = 1/T_s$ is the frequency spacing between adjacent subcarriers. After performing discrete Fourier transforms (DFT) on the time-domain OFDM symbols, the reference signal model in the subcarrier domain can be expressed as:

$$X_{\text{ref}} = [X_0, \ldots, X_l, \ldots, X_{L-1}]^{\text{T}}, \tag{5}$$

where superscript "T" indicates matrix transpose, and

$$X_l = \text{DFT}[d_l(n)] = \left[C_{l,0}, \ldots, C_{l,k}, \ldots, C_{l,N_s-1}\right]^{\text{T}}. \tag{6}$$

Similarly, under the assumption that the phase rotation caused by clutter or target Doppler shift is negligible within an OFDM symbol [14], the surveillance signal of (2) in the subcarrier domain can be expressed as:

$$\mathbf{Y}_{\text{surv}} = \begin{bmatrix} Y_{0,0} & \cdots & Y_{0,k} & \cdots & Y_{0,N_s-1} \\ \vdots & \ddots & \vdots & \ddots & \vdots \\ Y_{l,0} & \cdots & Y_{l,k} & \cdots & Y_{l,N_s-1} \\ \vdots & \ddots & \vdots & \ddots & \vdots \\ Y_{L-1,0} & \cdots & Y_{L-1,k} & \cdots & Y_{L-1,N_s-1} \end{bmatrix}, \tag{7}$$

where each column vector $\mathbf{Y}_k = \left[Y_{0,k}, \ldots, Y_{l,k}, \ldots, Y_{L-1,k}\right]^{\text{T}}$ can be expressed as:

$$\mathbf{Y}_k = \sum_{i=0}^{N_c} a_i^{\text{clu}} e^{-j2\pi \Delta f \tau_i^{\text{clu}}} \mathbf{Q}_{i,k} + \sum_{q=1}^{N_q} b_q^{\text{tar}} e^{-j2\pi \Delta f \tau_q^{\text{tar}}} \mathbf{U}_{q,k} + V_k, \tag{8}$$

with

$$\mathbf{Q}_{i,k} = \left[C_{0,k}, \ldots, C_{l,k}, \ldots, C_{L-1,k} \right]^{\text{T}}, \tag{9}$$

$$\mathbf{U}_{q,k} = \left[e^{j2\pi f_q \left(T_g + \tau_q^{\text{tar}} \right)}, \ldots, e^{j2\pi f_q \left(l T_s + T_g + \tau_q^{\text{tar}} \right)}, \ldots, e^{j2\pi f_q \left((L-1) T_s + T_g + \tau_q^{\text{tar}} \right)} \right]^{\text{T}} \odot \mathbf{Q}_{i,k}, \tag{10}$$

$$\mathbf{V}_k = \left[V_{0,k}, \cdots, V_{l,k}, \cdots, V_{L-1,k} \right]^{\text{T}}, \tag{11}$$

and $\odot$ stands for the Hadamard product.

Basing on the sparsity of each subcarrier-domain data in (8), the ES-based SR model is established in [23], by extracting only the data carried by all ESs to generate the RD map and its dimension of sparse dictionary is related to the number of delay-Doppler grids and the number of total samples carried by all ESs.

3 Proposed approaches

In this section, we first introduce the principle of the proposed AES-based SR model. Then, the reconstruction algorithm AES-COMP for AES model will be presented. Finally, in order to improve the target detection performance of the AES model for PBR with lower-SCR target and further reduce the computational complexity, we propose the stepwise estimation methods based on AES (AES-S) to achieve target detection.

3.1 Sparse representation based on AES

According to (8), the vector $\mathbf{Y}_k$ is composed of finite clutter and target components. Therefore, each ES vector of the PBR signal is sparse. Based on this, if we sum and average the data carried by all ESs vectors, the obtained data should also be sparse. This is core of our proposed AES-based SR model. The AES-based SR model can reduce the dimension of sparse dictionary. The processing flow of AES can be summarized in the following steps. First, transform the surveillance signal data to ES domain by performing DFT on each time-domain OFDM symbol. Second, obtain the data in AES domain by summing and averaging the data carried by all ESs vectors. The AES-based SR model is deduced in detail as follows.

Based on (8), the data carried by all ES vectors is summed and averaged to obtain:

$$\begin{aligned}
\mathbf{Y}_{\text{surv\_AES}} &= \left(\sum_{k=N_1}^{N_1+N_u-1} \right) / N_u \\
&= \sum_{i=0}^{N_c} a_i^{\text{clu}} \left(\sum_{k=N_1}^{N_1+N_u-1} \frac{e^{-j2\pi \Delta f \tau_i^{\text{clu}}}}{N_u} \mathbf{Q}_{i,k} \right) \\
&\quad + \sum_{q=1}^{N_q} b_q^{\text{tar}} \left(\sum_{k=N_1}^{N_1+N_u-1} \frac{e^{-j2\pi \Delta f \tau_q^{\text{tar}}}}{N_u} \mathbf{U}_{q,k} \right) + \sum_{k=N_1}^{N_1+N_u-1} \frac{1}{N_u} V_k,
\end{aligned} \tag{12}$$

where N_1 and N_u represent the starting and total number of averaged ES, respectively. Obviously, $\mathbf{Y}_{\text{surv\_AES}}$ is composed of three components related to clutter returns, target echoes and noise, respectively. Moreover, for the component of clutter returns we have:

$$\mathbf{S}_i^{\text{clu}} = \sum_{k=N_1}^{N_1+N_u-1} \frac{e^{-j2\pi\Delta f \tau_i^{\text{clu}}}}{N_u} \mathbf{Q}_{i,k}. \tag{13}$$

For the component of each target echo, we have:

$$\mathbf{S}_q^{\text{tar}} = \sum_{k=N_1}^{N_1+N_u-1} \frac{e^{-j2\pi\Delta f \tau_q^{\text{tar}}}}{N_u} \mathbf{U}_{q,k}. \tag{14}$$

Then,

$$\begin{aligned}
\mathbf{Y}_{\text{surv AES}} &= \sum_{i=0}^{N_c} a_i^{\text{clu}} \mathbf{S}_i^{\text{clu}} + \sum_{q=1}^{N_q} b_q^{\text{tar}} \mathbf{S}_q^{\text{tar}} + \sum_{k=N_1}^{N_1+N_u-1} \frac{1}{N_u} \mathbf{V}_k \\
&= \sum_{i=0}^{N_c} a_i^{\text{clu}} \mathbf{S}_i^{\text{clu}} + \sum_{q=1}^{N_q} b_q^{\text{tar}} \mathbf{S}_q^{\text{tar}} + \mathbf{e}_{\text{AES}},
\end{aligned} \tag{15}$$

which shows that the received signal $\mathbf{Y}_{\text{surv\_AES}}$ can be modelled as a linear combination of the target signal $\mathbf{S}_q^{\text{tar}}$ and $\mathbf{S}_i^{\text{clu}}$ the clutter signal. Moreover, both $\mathbf{S}_q^{\text{tar}}$ and $\mathbf{S}_i^{\text{clu}}$ are time- and frequency-shifted versions of $\mathbf{S}_0^{\text{clu}}$ multiplied by complex coefficients that are related to the size, shape and location of various scatters, where the signal $\mathbf{S}_0^{\text{clu}}$ is the data processed by superposition and averaging of illumination waveforms in the ES domain. Finally, since the number of targets and clutter in a real scene is limited in our whole surveillance area, the received signal $\mathbf{Y}_{\text{surv\_AES}}$ is sparse in the delay-Doppler domain and it can be modelled by:

$$\mathbf{Y}_{\text{surv\_AES}} = \mathbf{A}_{\text{AES}} \boldsymbol{\alpha} + \mathbf{e}_{\text{AES}}. \tag{16}$$

In (16), if $\mathbf{A}_{\text{AES}}$ is known, we can recover vector $\boldsymbol{\alpha}$ by solving the problem:

$$\boldsymbol{\alpha} = \underset{\boldsymbol{\alpha}}{\operatorname{argmin}} \left\| \mathbf{Y}_{\text{surv\_AES}} - \mathbf{A}_{\text{AES}} \boldsymbol{\alpha} \right\|. \tag{17}$$

Unfortunately, the calculation of $\mathbf{A}_{\text{AES}}$ and solving (17) are impractical because $\mathbf{A}_{\text{AES}}$ is unknown and depends on $M = N_c + N_q + 1$, τ_i^{clu}, τ_q^{tar} and f_q which are all unknown parameters. Fortunately, we can construct sparse dictionary by discretizing search space in practical application. Particularly, expected time delays in $(0 : T_0 : \tau_{\max})$ and Doppler frequencies in $(-f_{\max} : f_{\text{res}} : f_{\max})$ are discretized into I and J grids first, where the frequency resolution $f_{\text{res}} = 2f_{\max}/J$ depends on the number of grid points J. Then, we can extend $\mathbf{A}_{\text{AES}}$ to $\boldsymbol{\Psi}_{\text{AES}}$ by using these grid samples, and the SR model based on AES in (16) can be rewritten as:

$$\mathbf{Y}_{\text{surv\_AES}} = \mathbf{\Psi}_{\text{AES}}\boldsymbol{\beta} + \mathbf{e}_{\text{AES}}, \tag{18}$$

where $\mathbf{\Psi}_{\text{AES}} \in \mathbb{C}^{\mathbb{L}*\mathbb{IJ}}$ is named as the overcomplete sparse dictionary. Considering that the number of echo signals in the surveillance signal is limited, the parameter estimation problem of PBR can be transformed to the sparse signal reconstruction problem as:

$$\min_{\boldsymbol{\beta}} \|\boldsymbol{\beta}\|_1 \quad \text{s.t.} \quad \left\|\mathbf{Y}_{\text{surv\_AES}} - \mathbf{\Psi}_{\text{AES}}\boldsymbol{\beta}\right\|_2 \le \varepsilon, \tag{19}$$

where ε and $\boldsymbol{\beta}$ are the regulating parameter and the vectorized range-Doppler map, respectively. By comparing different SR models, it is worth noting that the matrix dimensions of sparse dictionaries for time-domain, ES-domain and AES-domain SR models are $LN_e \times JI$, $LN_u \times JI$ and $L \times JI$, respectively. It is obvious that when the delay grids I and Doppler grids J are the same, the AES-based SR model proposed has the smallest number of dictionary rows, and the matrix dimensionality is also the smallest. Therefore, the calculation speed of the AES-based SR model proposed in this paper will be significantly accelerated. More comparisons of AES algorithm and other SR models are given in Part D of Sect. 4, including the computation complexity and the minimum dictionary dimension required to detect the target at different signal-to-noise ratio (SNR).

3.2 AES-COMP algorithm

There are many algorithms to achieve the solution in (19). In general, OMP algorithm [28] is widely used because of its high computational efficiency and easy implementation. Therefore, we adopt the OMP algorithm, to the sparse matrix recovery problem in (19). The basic idea of the OMP algorithm is to sequentially find the support set of the measured signal and then project it on the atoms selected from the sparse dictionary. In (18), the observation vector $\mathbf{Y}_{\text{surv\_AES}}$ and sparse dictionary $\mathbf{\Psi}_{\text{AES}}$ are complex-valued, so we extend the OMP algorithm to the complex domain, i.e. AES-COMP. Specifically, we rewrite (18) as:

$$\mathbf{Y} = \begin{bmatrix} \Re\left(\mathbf{Y}_{\text{surv\_AES}}\right) \\ \Im\left(\mathbf{Y}_{\text{surv\_AES}}\right) \end{bmatrix} = \tilde{\mathbf{\Psi}}\tilde{\boldsymbol{\beta}} + \tilde{\boldsymbol{e}}, \tag{20}$$

where $\Re(.)$ and $\Im(.)$ are the real and imaginary parts, respectively, and

$$\tilde{\mathbf{\Psi}} = \begin{bmatrix} \Re(\mathbf{\Psi}_{\text{AES}}) & -\Im(\mathbf{\Psi}_{\text{AES}}) \\ \Im(\mathbf{\Psi}_{\text{AES}}) & \Re(\mathbf{\Psi}_{\text{AES}}) \end{bmatrix}, \tilde{\boldsymbol{\beta}} = \begin{bmatrix} \Re(\boldsymbol{\beta}) \\ \Im(\boldsymbol{\beta}) \end{bmatrix}, \tilde{\boldsymbol{e}} = \begin{bmatrix} \Re(\boldsymbol{e}_{\text{AES}}) \\ \Im(\boldsymbol{e}_{\text{AES}}) \end{bmatrix}. \tag{21}$$

Since all columns of $\mathbf{\Psi}_{\text{AES}}$ are the time- and frequency-shifted versions of transmitted signal, all of them have the same norm, and based on (21), all columns of $\tilde{\mathbf{\Psi}}$ also have equal norms [21]. Thus, we can use AES-COMP to extract $\tilde{\boldsymbol{\beta}}$ of (20). The steps of AES-COMP algorithm are provided in Algorithm 1.

Algorithm 1 AES-COMP Algorithm

1: **Input:** $\tilde{\boldsymbol{\Psi}}, \mathbf{Y}$, iteration number W
2: **Output:** $\boldsymbol{\beta}$
3: **Initialization:** $w = 1, \mathbf{r}_0 = \mathbf{Y}, \Lambda_0 = \varnothing, \mathbf{x}_0 = 0$
4: **Identification**
     • Find index $\lambda_w = \underset{j=1,2,\cdots,JI}{\operatorname{argmax}} \left| \left\langle \mathbf{r}_{w-1} | \tilde{\boldsymbol{\Psi}}_j \right\rangle \right|$
5: **Agumentation**
     • Update $\Lambda_w = \Lambda_{w-1} \cup \lambda_w$
     • Update $\mathbf{x}_w = \left[\mathbf{x}_{w-1}, \tilde{\boldsymbol{\Psi}}_{\lambda_w} \right]$
6: **Residual Update**
     • Solve the Least Squares Problem: $\tilde{\boldsymbol{\beta}}_w = \left(\mathbf{x}_w^{\mathbf{H}} \mathbf{x}_w \right)^{-1} \mathbf{x}_w^{\mathbf{H}} \mathbf{Y}$
     • Calculate new approximation: $\gamma_w = \mathbf{x}_w \tilde{\boldsymbol{\beta}}_w$
     • Update the residual vector: $\mathbf{r}_w = \mathbf{Y} - \gamma_w$
7: Increment w, and repeat from step 4 if $w \leq W$

3.3 AES-based stepwise algorithm

As described in part A of Sect. 3, since the surveillance signal in (15) consists of a few targets and clutter, we can describe the surveillance signal as:

$$\mathbf{Y}_{\text{surv\_AES}} = \mathbf{Y}_{\text{clu}} + \mathbf{Y}_{\text{tar}+\mathbf{e}_{\text{AES}}}, \tag{22}$$

where the clutter $\mathbf{Y}_{\text{clu}}$ and target $\mathbf{Y}_{\text{tar}}$ can be estimated using AES-COMP. However, in order to successfully detect the weak targets in the surveillance signal, the sparse dictionary $\boldsymbol{\Psi}_{\text{AES}}$ needs to have a very large dimension, which will bring a lot of computation to the algorithm. In addition, if the SNR of targets are very low, even if the dimension of dictionary $\boldsymbol{\Psi}_{\text{AES}}$ is large enough, the target parameters estimated by AES-COMP algorithm may be inaccurate. Since the power of clutter is much stronger than that of target echo, the clutter signal is estimated first during sparse reconstruction, followed by the target echo. In addition, the estimated clutter coefficients are distributed on the zero Doppler of RD map and can be easily distinguished from the target. Thus, we propose a stepwise algorithm based on AES sparse model (AES-S). Specifically, we first use the AES-based SR model to obtain clutter coefficients $\hat{\mathbf{a}}_p^{\text{clu}} = \left[\hat{\mathbf{a}}_1^{\text{clu}}, \dots, \hat{\mathbf{a}}_{N_p}^{\text{clu}} \right]$ and time delays $\hat{\boldsymbol{\tau}}_p^{\text{clu}} = \left[\hat{\boldsymbol{\tau}}_1^{\text{clu}}, \dots, \hat{\boldsymbol{\tau}}_{N_p}^{\text{clu}} \right]$ of clutter. Then, we subtract the clutter component $\hat{\mathbf{Y}}_{\text{clu}}$ from the surveillance signal $\mathbf{Y}_{\text{surv}}$ according to $\hat{\mathbf{a}}_p^{\text{clu}}$ and $\hat{\boldsymbol{\tau}}_p^{\text{clu}}$. Finally, we can rewrite (22) as:

$$\hat{\mathbf{Y}}_{\text{tar\_AES}} = \mathbf{Y}_{\text{surv}} - \hat{\mathbf{Y}}_{\text{clu}}, \tag{23}$$

where $\hat{\mathbf{Y}}_{\text{tar\_AES}}$ includes the target echo and noise. However, the noise in $\hat{\mathbf{Y}}_{\text{tar\_AES}}$ is not the main factor affecting the detection results during target detection, so we can achieve target detection by computing CAF between the $\hat{\mathbf{Y}}_{\text{tar\_AES}}$ and the reference signal.

For the estimation of clutter, basing on the fact that the clutter is always around the zero-frequency grid and clutter with different time delays but at the same subcarrier is totally correlated, we can generate sparse dictionary $\boldsymbol{\Psi}_{\text{AES\_S}}$ with small RD range. Here, we consider all delays in the interval $\left(0, \tau_{\text{AES\_S}} \right)$ as $I_{\text{AES\_S}}$ time grids and discretize the Doppler frequencies in the interval $\left(-f_{\text{AES\_S}} : f_{\text{AES\_S}} \right)$ into $J_{\text{AES\_S}}$ frequency

grids. Notably, since the AES-S algorithm only needs to consider the Doppler range of clutter at the first step, and the clutter is around zero frequency, the Doppler grid set by AES-S algorithm is much smaller than that set by the AES-based SR model. Therefore, the AES-S algorithm will further reduce the computational load when detecting weak targets. For the suppression of clutter components, since we can remove the clutter components in the subcarrier or time domains, respectively, the AES-S algorithm for target information estimation can be implemented in the following two ways.

1. AES-S by removing clutter in the subcarrier domain (AES-S-C)

   Based on the $\hat{\mathbf{a}}_p^{\text{clu}}$ and $\hat{\boldsymbol{\tau}}_p^{\text{clu}}$ of clutter already obtained, we can obtain the clutter $\hat{\mathbf{Y}}_{\text{clu\_C}} = \left[\hat{\mathbf{Y}}_{\text{clu\_C},0}, \ldots, \hat{\mathbf{Y}}_{\text{clu\_C},l}, \ldots, \hat{\mathbf{Y}}_{\text{clu\_C},L-1}\right]^{\text{T}}$ in the subcarrier domain, where $\hat{\mathbf{Y}}_{\text{clu\_C},l}$ can be expressed as:

$$
\hat{\mathbf{Y}}_{\text{clu\_C},l} = \left[\sum_{p=1}^{N_p} \hat{a}_p^{\text{clu}} C_{l,0}, \ldots, \sum_{p=1}^{N_p} \hat{a}_p^{\text{clu}} e^{j2\pi k \Delta f \tau_p^{\text{clu}}} C_{l,k}, \ldots, \right.
$$
$$
\left. \sum_{p=1}^{N_p} \hat{a}_p^{\text{clu}} e^{j2\pi (N_s-1)\Delta f \tau_p^{\text{clu}}} C_{l,N_s-1}\right]^{\text{T}}. \tag{24}
$$

   Then, we can obtain the output signal $\hat{\mathbf{Y}}_{\text{tar\_C}} = \left[\hat{\mathbf{Y}}_{\text{tar\_C},0}, \ldots, \hat{\mathbf{Y}}_{\text{tar\_C},l}, \ldots, \hat{\mathbf{Y}}_{\text{tar\_C},L-1}\right]^{\text{T}}$ in the subcarrier domain after clutter cancellation, where $\hat{\mathbf{Y}}_{\text{tar\_C},l} = \left[D_{l,0}, \ldots, D_{l,k}, \ldots, D_{l,N_s-1}\right]^{\text{T}}$ can be expressed as:

$$
\hat{\mathbf{Y}}_{\text{tar\_C},l} = \mathbf{Y}_l - \hat{\mathbf{Y}}_{\text{clu\_C},l}, \tag{25}
$$

   where $\mathbf{Y}_l = \left[Y_{l,0}, \ldots, Y_{l,k}, \ldots, Y_{l,N_s-1}\right]^{\text{T}}$ is the lth-row vector of (7). Finally, we perform CAF between the output signal $\hat{\mathbf{Y}}_{\text{clu\_C}}$ and the reference signal $\mathbf{X}_{\text{ref}}$ in the subcarrier domain to obtain target information. The CAF in subcarrier domain can be written as:

$$
\chi[m,p] = \sum_l^{L_{\text{CAF}}} e^{-j2\pi pl/L_{\text{CAF}}} \sum_{k=0}^{N_s-1} D_{l,k} C_{l,k}^* e^{j2\pi pkm/N_s}, \tag{26}
$$

   where L_{CAF} is the required number of symbols for CAF. The parameter m is the delay bin representing the delay $\tau = mT_0$ and p is the Doppler bin representing the Doppler frequency $f = p/T_0 N_{\text{int}}$, where $N_{\text{int}} = L_{\text{CAF}} N_e$ is the number of integrated samples. In addition, we can also do stepwise processing in the time domain, and the specific steps are as follows.

2. AES-S by removing clutter in the time domain (AES-S-T)

   Like the steps of AES-S-C algorithm, we first obtain the clutter signal $\hat{y}_{\text{clu\_T}}$ in time domain through $\hat{\mathbf{a}}_p^{\text{clu}}$ and $\hat{\boldsymbol{\tau}}_p^{\text{clu}}$,

$$\hat{y}_{\text{clu\_T}}(t) = \sum_{p=1}^{N_p} \hat{a}_p^{\text{clu}} d\left(t - \hat{\tau}_p^{\text{clu}}\right). \tag{27}$$

Then, the output signal $\hat{y}_{\text{tar\_T}}$ can be written as:

$$
\begin{aligned}
\hat{y}_{\text{tar\_T}}(t) &= y_{\text{surv}}(t) - \hat{y}_{\text{clu\_T}}(t) \\
&= y_{\text{surv}}(t) - \sum_{p=1}^{N_p} \hat{a}_p^{\text{clu}} d\left(t - \hat{\tau}_p^{\text{clu}}\right).
\end{aligned}
\tag{28}
$$

Finally, we perform CAF in time domain to estimate targets. The CAF can be expressed as:

$$\chi[m,p] = \sum_{n=0}^{N_{\text{int}}} \hat{y}_{\text{tar\_T}}[n] x_{\text{ref}}^*[n-m] e^{-j2\pi pn/N_{\text{int}}}, \tag{29}$$

where $x_{\text{ref}}[n]$ and $\hat{y}_{\text{tar\_T}}[n]$ are the sampled reference signal in (1) and output signal in (28), respectively. By the way, the AES-S-T method can be used for other types of opportunity illuminators, not limited to OFDM signals.

4 Simulation analysis

In this section, we first present the target detection results of the proposed algorithms in simulated scenarios and compare them with the traditional clutter suppression method. Then, we use four metrics to mathematically analyse the detection performance of the proposed algorithms.

4.1 Simulation setting

Here, we evaluate the performance of the proposed algorithms based on PBR using DRM-based OFDM signal. To evaluate the detection ability of the proposed algorithm more intuitively in real situations, we consider a multitarget simulation scenario containing several targets with different SNRs in this section. In the simulation, the transmit signal is generated according to the standard of DRM signal in mode B and is used as a reference channel signal, which is clean and free of noise. The bandwidth of the OFDM signal is 9.7 kHz, the number of ESs is 207, $\Delta f = 46.875$ Hz, $N_s = 256$ and $N_g = 64$. The time-domain sample interval T_0 is 1/12000 s. In total, 2500 OFDM symbols are used to generate the dictionaries Ψ_{AES} and $\Psi_{\text{AES\_S}}$, respectively. The Doppler shift range of sparse dictionary Ψ_{AES} is set to $-18.6 \sim 18.6$ Hz, where the Doppler resolution is 0.15 Hz. And the maximum delay of the target does not exceed the number of CPs of the OFDM symbol, so the delay range of sparse dictionary Ψ_{AES} is set to 0:1:40 (samples). Since only zero-frequency clutter is considered, the Doppler grid of $\Psi_{\text{AES\_S}}$ is only set at 0 Hz, and the delay range is consistent with that of Ψ_{AES}. The RD-domain data will be obtained after CAF processing where the coherent processing interval is about 13.6 s.

In the surveillance channel, 13 stationary scatterers are used to simulate clutter. The clutter-to-noise ratios (CNRs) of the simulated zero-Doppler clutter are (70:-5:10) dB. Besides, the corresponding bistatic delay bins are (0:1:12) samples. In addition, the surveillance channel contains 5 targets, and the values of their bistatic delay bin, Doppler

shift and SNR parameters are listed in Table 1. Furthermore, we assume that both the target and the clutter are point scattered, and the thermal noise is modelled as complex white Gaussian noise.

4.2 Simulation results

We first assess the effect of clutter on target detection. Figure 2 shows the RD map of received signal in simulation scenario of Table 1 without using any clutter cancellation method. As shown in Fig. 2, the simulated targets are completely masked by clutter, and only clutter with very strong CNR can be seen. This phenomenon indicates the necessity of clutter suppression in PBR. Therefore, the target detection of PBR needs various interference cancellation algorithms as remedial measures. Because the authors of [12] have demonstrated that the ECA-B algorithm has good target detection performance, we use the ECA-B algorithm as a benchmark to compare with the algorithm proposed in this paper.

Now, we evaluate the target detection and interference cancellation performance of our proposed algorithm in a multitarget scenario as shown in 1. At the same time, we also compare the performance of our proposed algorithm with the ECA-B algorithm in target detection and interference cancellation. Figure 3a shows the RD map after clutter suppression using ECA-B. Obviously, the targets T_1 and T_4, which have low Doppler frequencies, are eliminated during the clutter suppression process. Moreover, the strong target T_2 creates side lobes around the target T_3, resulting in some SNR

Table 1 Target parameters of the simulation

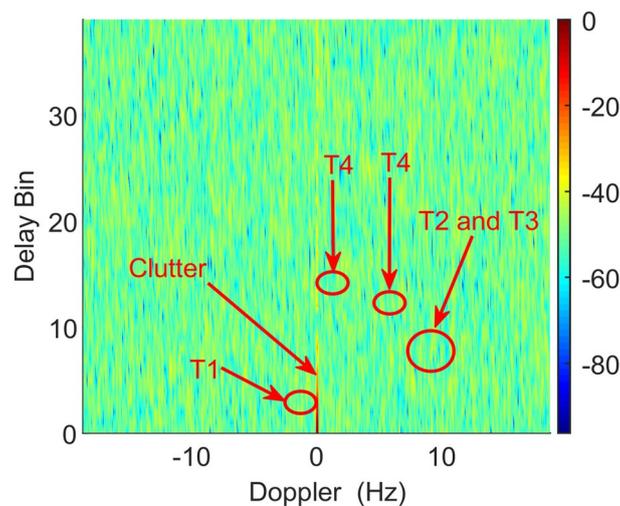| Target	T_1	T_2	T_3	T_4	T_5
Delay (samples)	3	8	8	15	12
Doppler (Hz)	− 0.3	9	8.4	0.45	6
SNR (dB)	− 6	10	0	− 22	− 10

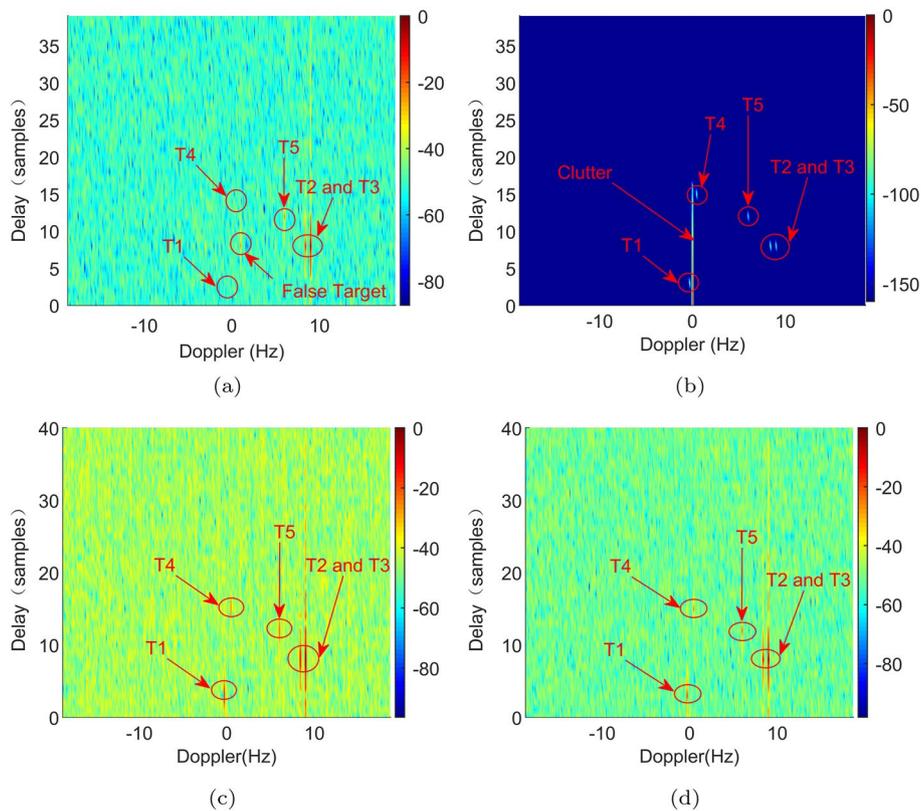**Fig. 2** RD map before clutter suppression

Fig. 3 Simulated results obtained by different methods in the simulated multitarget scenario of Table 1. **a** RD map obtained by ECA-B algorithm. **b** RD map obtained by AES algorithm. **c** RD map obtained by AES-S-C algorithm. **d** RD map obtained by AES-S-T algorithm

loss at T_3. Furthermore, the algorithm generates some false targets when detecting multitarget scenarios, which will affect the subsequent operation of PBR. Figure 3b shows the RD map obtained using the AES model. We have noticed that there are 5 peaks in the RD map, and the results are consistent with the given target parameters, which proves the correctness of the algorithm. The algorithm can detect all echoes, including targets and clutter, in a uniform manner without prior knowledge of the clutter location or statistics. Furthermore, the target T_1, which cannot be detected using the ECA-B, is detected, and located by AES. Figure 3c,d shows the RD maps using the AES-S-T and the AES-S-C algorithms, respectively. It can be seen that both algorithms can successfully detect the targets, which are given in Table 1. The reason that the target T_1 and T_4 can be detected using these two algorithms is as follows. In the process of eliminating clutter, we only eliminate the zero-frequency clutter but do not eliminate the signals near the zero frequency at the same time.

Next, we demonstrate the unique high range resolution capability of the AES algorithm. To illustrate the high range resolution capability of AES, we add a new target T_6 near T_5 with the same Doppler shift. Moreover, T_6 and T_5 are only 1 time delay away from each other. Figure 4a, b shows the RD maps of the detected targets using ECA-B and AES, respectively. We observe that T_6 and T_5 are correctly resolved and located using the AES method. However, only the peak of the strong target T_6 is visible on
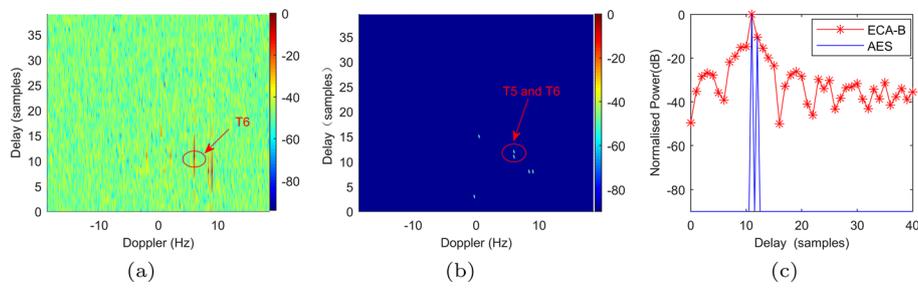
Fig. 4 Simulation detection results of RD maps comparing the high range resolution capability of different algorithms. **a** RD map obtained by ECA-B algorithm. **b** RD map obtained by AES algorithm. **c** Range profile at Doppler 6Hz
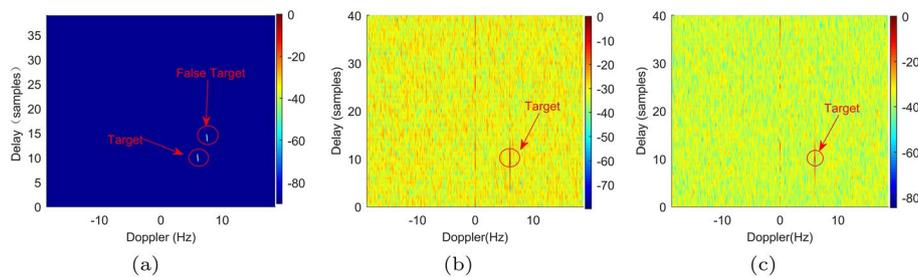

Fig. 5 Simulation detection results of the single target with low SCR by different algorithms. **a** RD map obtained by AES algorithm. **b** RD map obtained by AES-S-C algorithm. **c** RD map obtained by AES-S-T algorithm

the RD map by using ECA-B algorithm, and the weak target T_5 is masked by T_6. It is worth noting that we do not show the clutter in Fig. 4b in order to highlight the target. For a more visual comparison, Fig. 4c shows two profiles of the ECA-B and AES along the range dimension at Doppler 6 Hz. It can be seen that the target estimated by the ECA-B method suffers from a severe main lobe split, which affects the detection of adjacent target.

Finally, we investigate the target detection and interference cancellation performance of AES-S-T and AES-S-C in the low-SCR case and compare them with the AES algorithm. Here, we consider a simulated scenario in a single-target scenario with SNR of -30 dB, namely low SCR of -100 dB. Moreover, clutter parameters here are consistent with the clutter parameters in Table 1. The simulation results are shown in Fig. 5. From the simulation results, we can see that another peak that cannot be matched with the target position appears when using the AES sparse model to detect target, and this peak is not very different from the target peak, which may lead us to misidentify the peak as target, i.e. a false target. However, the AES-S-T and AES-S-C methods can effectively detect weak targets with very low SCR. In addition, due to the inevitable estimation error of the AES-COMP algorithm, it leads to some residual clutter in the AES-S algorithm at 0Hz. Fortunately, the tolerable error does not affect target detection.

4.3 Performance assessment

In this subsection, we mathematically analyse the detection ability of the proposed algorithm in the presence of interference. There are various metrics that can be used to

measure target detection performance. In this paper, we use the following three metrics. The first metric is PSLR, which can represent the ability of the PBR to detect weak targets [30]. It gives the ratio between the highest sidelobes and the peak. If detecting targets in the presence of strong clutter, PSLR is critical and must be kept low to prevent mistaking one side lobe as another small target. Therefore, the lower the PSLR, the better the detection performance of the algorithm. PSLR in dB scale is defined as:

$$\text{PSLR} = 20\log\left(\max_{m\in D,p\in F}(|\beta[m,p]|)/|\beta[m_0,p_0]|\right), \tag{30}$$

where m_0 and p_0 are the range bin and Doppler bin of target, respectively. The parameters D and F, respectively, define the set of range bins and Doppler bins except for main lobe in the RD map. The second metric is ISLR, which is a measure of the energy distributed in the side lobes [30]. It gives the ratio between the cumulative and peak values of the side lobe. It is important to use a low ISLR to keep weak targets visible. So, the lower the ISLR of the algorithm, the better the performance. The ISLR in dB scale is defined as:

$$\text{ISLR} = 20\log\frac{\sum_{m\in D,f\in F}|\beta[m,p]|^2}{\sum_{m\notin D,f\notin F}|\beta[m,p]|^2}. \tag{31}$$

The third indicator is Err [31], which is a measure of the accuracy of parameter estimation and can be defined as:

$$\text{Err} = \|\beta - \beta_0\|_2/\|\beta_0\|_2, \tag{32}$$

where β_0 and β are the real and estimated sparse coefficients in the RD map, respectively. The smaller the ERR value, the higher the estimation accuracy of the target parameters after processing by the algorithm.

To quantitatively evaluate different algorithms by the above metrics, we change the target SNR from −20 to 10 dB with step size 3 dB, and the clutter environment is set up the same way for the multitarget scene. After the clutter suppression and CAF calculation, the PSLR, ISLR and Err of target are obtained from the RD maps, which represents the clutter suppression performance. In total, 100 Monte Carlo (MC) simulations are performed for each algorithm at each SNR. We insert one single target to calculate PSLR and ISLR, while arbitrarily selecting three targets to obtain results of Err.

We know that in order to prevent weak targets from being covered by side lobes of strong targets, the lower the PSLR and ISLR, the better the performance. We depict the relationship between the three metrics and the target SNR using different algorithms in Fig. 6. We observe that our proposed three algorithms outperform the traditional algorithm ECA-B in terms of PSLR and ISLR, and the AES algorithm has the best performance in all aspects. Moreover, the ISLR of AES-S-T is slightly lower than that of AES-S-C. This is caused by the fact that the noise floor of AES-S-C is higher than that of AES-S-T. Therefore, the AES-S-T algorithm performs slightly better than the AES-S-C algorithm. When we analyse the Errs of four algorithms in the case of multiple targets, it is found that the AES algorithm has the smallest Err values, which is almost close to zero. And we also find that the Err values of AES-S-T and AES-S-C are almost the same. The reason for this phenomenon is that the Err of AES-S-T and AES-S-C depends
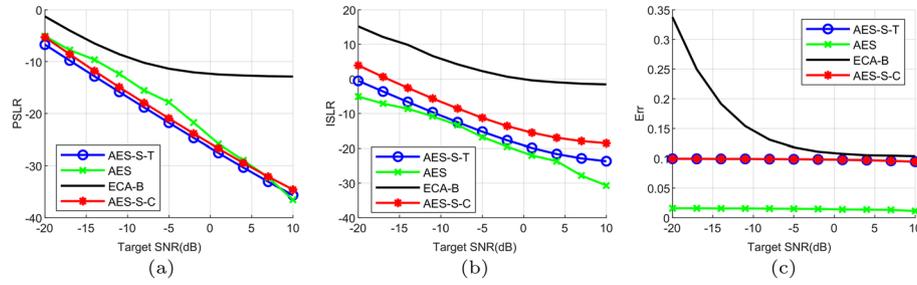
Fig. 6 Performance comparisons of AES, ECA-B, AES-S-C and AES-S-T. **a** PSLR. **b** LSLR. **c** Err

Table 2 Computational complexity in terms of complex multiplications

Algorithm	Clutter suppression	Overcomplexity
AES-S-T	$C_{\text{T\_SR}} = O\left(4LJ_{\text{AES\_S}}I_{\text{AES\_S}}W_{\text{AES\_S}}\right)$	$C_{\text{T\_SR}} + C_{\text{T\_CAF}}$
AES-S-C	$C_{\text{C\_SR}} = O\left(4LJ_{\text{AES\_S}}I_{\text{AES\_S}}W_{\text{AES\_S}}\right)$	$C_{\text{C\_SR}} + C_{\text{C\_CAF}}$
AES	0	$O(4LJIW)$

on the first step of the stepwise algorithm for clutter suppression operation, and both AES-S-T and AES-S-C clutter suppression operations are implemented using AES. So, they have the same degree of clutter suppression and the same reconfiguration accuracy of the target. This result is consistent with the conclusion in [23]. We further find that PSLR and ISLR are inversely proportional to the target SNR. When the target SNR increases gradually, PSLR and ISLR gradually decrease accordingly. Overall, the analysis results are consistent with the definitions of PSLR and ISLR, which further illustrates the correctness of the proposed algorithms.

4.4 Computational complexity

In this section, we investigate the computational complexity of the proposed algorithm. We first compare the complexity of the three algorithms proposed in this paper, where the computational complexity of the algorithms is measured by the number of complex multiplications. The computational complexities of the AES-S-T and AES-S-C algorithms come from the following two processing stages: clutter suppression and CAF calculation, where the computational complexity of CAF calculations in the time domain and subcarrier domain is

$$C_{\text{T\_CAF}} = N_e L_{\text{CAF}}\left(1.5\log_2 N_e + 0.5\log_2 L_{\text{CAF}} + 1\right), \tag{33}$$

$$C_{\text{C\_CAF}} = N_s L_{\text{CAF}}\left(1.5\log_2 N_s + 0.5\log_2 L_{\text{CAF}} + 1\right), \tag{34}$$

Table 2 summarizes the computational complexity of the proposed three algorithms.

Here, a specific comparison for computational complexity is given via the simulation parameters listed in Table 1. When introducing the AES-S-T and AES-S-C algorithms, we assume that the number of iterations $W_{\text{AES\_S}} = 20$, and the required number of symbols for CAF is $L_{\text{CAF}} = 512$. The overall computational complexities of the AES-S-T and AES-S-C are about 1.115×10^7 and 1.049×10^7, respectively. For

comparison, the computational complexity of AES is about 2.042×10^9. From the above results, we can see that the computational complexity of the AES-S algorithm is significantly lower than that of the AES-based SR model. Therefore, the AES-S algorithm proposed in this paper can not only achieve the detection of weak targets, but also further reduce the computational complexity.

  In addition, we compare the computational complexity of the AES-based SR model proposed in this paper with existing SR models, such as the time-domain SR model proposed in [21] and the ES-based SR model proposed in [23]. Table 2 shows that the main factor affecting the computational complexity is the dictionary's matrix dimension, when using the same sparse reconstruction algorithm. Also, as described in Section III-A, it is easy to understand that when the grid parameters (namely J and I) are defined, the sparse reconstruction algorithms' target detection ability will increase as the dictionary dimension gets larger (namely L gets larger). Therefore, we analyse the minimum number of L required by the three SR models to detect the target at different SNR in Fig. 7, where the parameters J and I for three SR models are consistent with the simulation part. As can be seen from the result in Fig. 7, the dimension of the AES algorithm is much smaller than that of the SR model in [21, 23], which means that the calculation speed can be correspondingly accelerated. Specifically, the calculation of the proposed AES-based model amount can be reduced by about 50% compared with the time-domain SR model in [21]. Compared with the ES-based SR model in [23], the computation of our proposed SR model can be reduced by about 46.97%. Therefore, the AES-domain SR model proposed in this paper can effectively reduce the computational compared with the existing SR models.
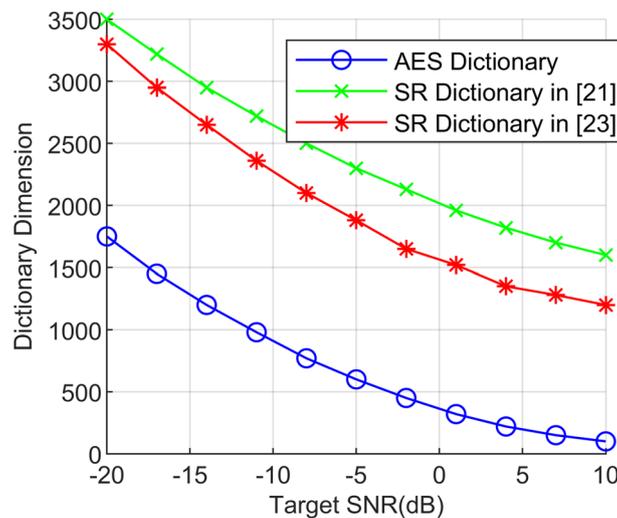

Fig. 7 Smallest dimension of the dictionary for different SR models while the number of delay-Doppler grids is determined

5 Experimental results

To further demonstrate the effectiveness of the proposed method in this paper, we use the measurement data for validation. The measured data is obtained from the detection experiment of DRM-based passive radar [32]. The effective bandwidth of the DRM broadcast signal received by this radar system is 9.7 kHz, and the operating frequency is 10 MHz. The transmitting station is in Qingdao, and the receiving station is located on the coast of Haiyang City, Hainan Province, China, with about 50 km between the receiving and transmitting stations. The receiving antenna is a linear array with 16 elements, and the transmitted signal mainly reaches the receiving array via the ground wave propagation mode. As the reference channel and the surveillance channel shares the same array, the receiving array beam is pointed to the direction of the transmitter and the target at the receiving side to obtain the reference signal and the surveillance channel signal, respectively.

Because the SCR of target is extremely low in the real situation, it may not be able to detect the target accurately by directly using the AES-based SR model with restricted dimension of sparse dictionary, and false targets will appear as shown in Fig. 5a. Therefore, we will directly use the AES-S-C and AES-S-T algorithms to detect target for the measured data. We set the Doppler shift range of distributed clutter dictionary from − 2 to 2 Hz, with adjacent intervals of 0.5 Hz. The delay bin for target is considered in the range of 0:1:64(samples). Since the truth location of target cannot be obtained in the real experiment as in the simulation experiment, we use the results after the ECA-B algorithm clutter suppression as a reference to validate the experiment.

The results of two measured data are shown in Figs. 8 and 9. Figures 8a and 9a show the RD maps of the measured data without clutter suppression. In these figures, the target cannot be identified at all and only strong clutter at zero frequency can be observed. Figures 8b and 9b present show the RD maps of measured data after clutter suppression by the ECA-B algorithm. As can be seen from the figures, the detected target Doppler frequencies of two sets of measured data are about − 3.6 Hz and 4.98 Hz, respectively. However, there is still a lot of residual clutter in the RD maps that have not been suppressed (mainly sea clutter). Figure 8c, d shows the target RD maps after using the AES-S-T and AES-S-C algorithms for the measured data I, respectively. We observe that the AES-S-T and AES-S-C algorithms are effective in detecting the targets in the measurement data. Similarly, the targets of measurement data II are also effectively detected in Fig. 9c, d.

For a more intuitive comparison, Figs. 8e and 9e show the normalized target range bin cuts of the two measurement sets after clutter suppression by the three algorithms. For the sake of better observation, we have selected only part of the normalized target range bin cuts. We find that the detection performance of the AES-S algorithm is better than the ECA-B algorithm. To make the results clearer, SNR values of the same target after different algorithms in Figs. 8e and 9e are shown in Table 3, which shows that the detection performance of the AES-S algorithm is better than the ECA-B algorithm.
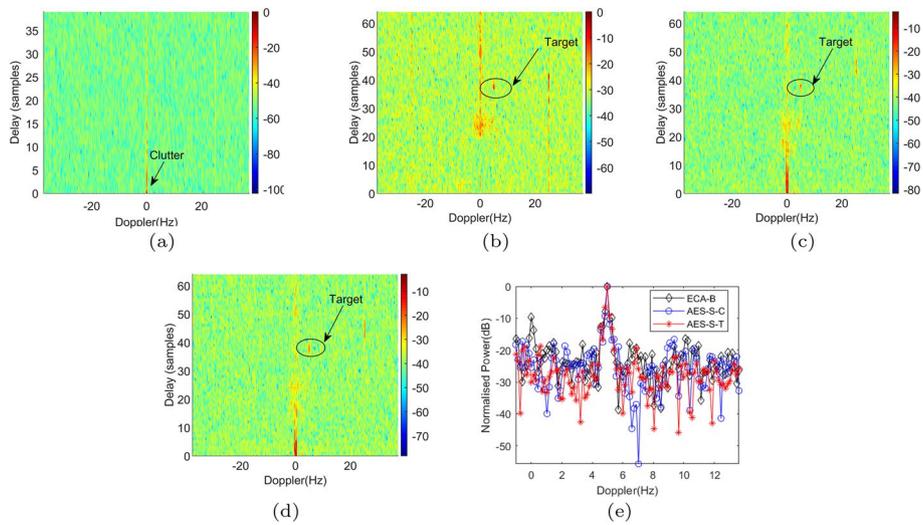
Fig. 8 Results of experimental data I. **a** RD map before clutter suppression. **b** RD map after clutter suppression by ECA-B algorithm. **c** Result of target extraction using AES-S-T method. **d** Result of target extraction using AES-S-C method. **e** Normalized target range bin cuts
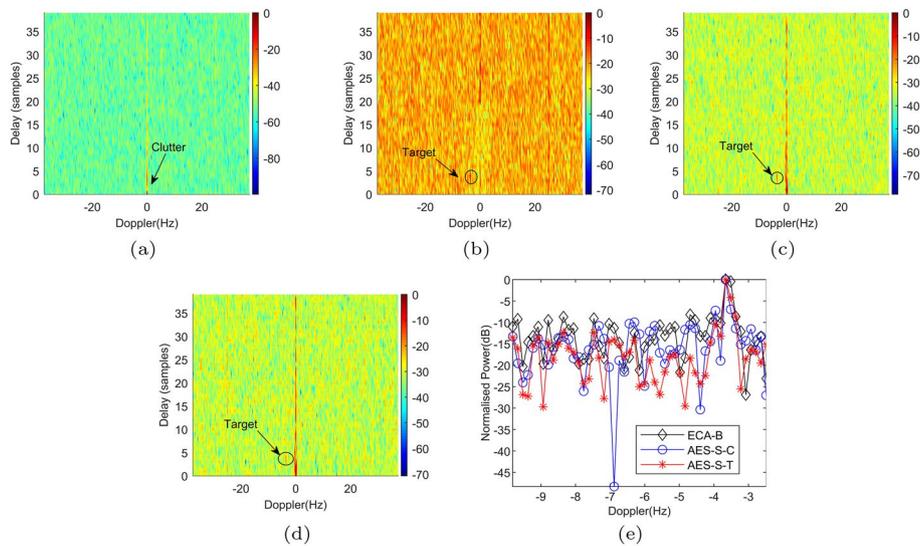

Fig. 9 Results of experimental data II. **a** RD map before clutter suppression. **b** RD map after clutter suppression by ECA-B algorithm. **c** Result of target extraction using AES-S-T method. **d** Result of target extraction using AES-S-C method. **e** Normalized target range bin cuts

Table 3 The target SNR using different algorithms

Algorithm	Experimental data I (dB)	Experimental data II (dB)
AES-S-T	24.48	17.91
AES-S-C	20.93	14.36
ECA-B	19.14	12.77

6 Conclusion

In this paper, to solve the high-dimensional problem of PBR target detection based on SR model, we first established an efficient and complexity-reduced SR model based on AES by using the sparsity of CP-OFDM-based PBR signal in each effective subcarrier channel. Then, we further proposed the AES-S-C and AES-S-T algorithms to solve the problem that the existing SR models still faces the problems of high computation and inaccurate target parameter estimation when detecting weak targets. By transforming the time delay estimation problem of clutter to the problem of the sparse signal representation, the proposed algorithms obtain the output signal after clutter cancellation with the clutter parameters estimated. We provide extensive simulation results to demonstrate the efficiency of the proposed algorithm in target detection. The metrics of PSLR, ISLR and Err are used to quantitatively measure the performance of algorithms. Results show that the proposed algorithms have lower PSLR, ISLR and Err. In addition, experiments with real PBR data in complex clutter environment demonstrate the effectiveness of the proposed algorithms. In future work, we will further verify the moving target detection performance of the algorithm in different clutter environments. In the future work, we will further study the improvement of sparse reconstruction algorithm, such as using the iterative shrinkage-thresholding-based algorithms, alternating direction method of multiplier-based algorithms and off-grid sparse reconstruction methods.

Date availability
The data that support the findings of this study are available from the corresponding author upon reasonable request.

Declarations

Competing interests
We declare that we have no financial and personal relationships with other people or organizations that can inappropriately influence our work and there is no professional or other personal interest of any nature or kind in any product, service and/or company that could be construed as influencing the position presented in or the review of the manuscript entitled.

References

1. G. Mazurek, Signal conditioning for DAB-illuminated passive radar. in *2021 Signal Processing Symposium (SPSympo)* (2021), pp. 193–196
2. G. Bournaka, M. Ummenhofer, D. Cristallini, J. Palmer, A. Summers, Experimental study for transmitter imperfections in DVB-T based passive radar. IEEE Trans. Aerosp. Electron. Syst. **54**(3), 1341–1354 (2018)
3. J.M. Thomas, H.D. Griffiths, C.J. Baker, Ambiguity function analysis of digital radio mondiale signals for hf passive bistatic radar. Electron. Lett. **42**(25), 1482–1483 (2006)
4. L. Gao, Z. Cao, M. Dai, J. Liu, L. Li, China digital radio (CDR) system and its application in emergency broadcasting. IEEE Trans. Broadcast. **65**(1), 187–191 (2019)
5. L. Storrer, H.C. Yildirim, M. Crauwels, Indoor tracking of multiple individuals with an 802.11ax wi-fi-based multi-antenna passive radar. IEEE J. Sel. **21–18**, 20462–20474 (2021)
6. H. Sun, D.K.P. Tan, Y. Lu, Aircraft target measurements using A GSM-based passive radar. in *Proceedings of IEEE Radar Conference Rome* (Italy, 2021), pp. 1–6
7. G. Fabrizio, F. Colone, P. Lombardo, A. Farina, Adaptive beamforming for high-frequency over-the-horizon passive radar. IET Radar, Sonar Navig. **3**(4), 384–405 (2009)

8. R. Tao, H.Z. Wu, T. Shan, Direct-path suppression by spatial filtering in digital television terrestrial broadcasting-based passive radar. IET Radar, Sonar Navig. **4**(6), 791–805 (2010)

9. H. Bolvardi, M. Derakhtian, A. Sheikhi, Dynamic clutter suppression and multitarget detection in a DVB-T-based passive radar. IEEE Trans. Aerosp. Electron. Syst. **53**(4), 1812–1825 (2017)

10. M. Meller, Cheap cancellation of strong echoes for digital passive and noise radars. IEEE Trans. Signal Process. **60**(5), 2654–2659 (2012)

11. X. Guan, D. Hu, L. Zhong, C. Ding, Strong echo cancellation based on adaptive block notch filter in passive radar. IEEE Geosci. Remote Sens. Lett. **12**(2), 339–343 (2014)

12. F. Colone, D.W. O'Hagan, P. Lombardo, C.J. Baker, A multistage processing algorithm for disturbance removal and target detection in passive bistatic radar. IEEE Trans. Aerosp. Electron. Syst. **45**(2), 698–722 (2009)

13. F. Colone, C. Palmarini, T. Martelli, E. Tilli, Sliding extensive cancellation algorithm for disturbance removal in passive radar. IEEE Trans. Aerosp. Electron. Syst. **52**(3), 1309–1326 (2016)

14. Z. Zhao, X. Wan, Q. Shao, Z. Gong, F. Cheng, Multipath clutter rejection for digital radio mondiale-based hf passive bistatic radar with OFDM waveform. IET Radar, Sonar Navig. **6**(9), 867–872 (2012)

15. M.A. Attalah, T. Laroussi, F. Gini, M.S. Greco, Range-doppler fast block LMS algorithm for a DVB-T-based passive bistatic radar. Signal Image Video Process **13**, 27–34 (2019)

16. L. Zheng, X. Wang, Super-resolution delay-doppler estimation for OFDM passive radar. IEEE Trans. Sign. Process. **65**(9), 2197–2210 (2017)

17. F. Soldovieri, R. Solimene, L. Lo Monte, M. Bavusi, A. Loperte, Sparse reconstruction from GPR data with applications to rebar detection. IEEE Trans. Instrum. Meas. **60**(3), 1070–1079 (2011)

18. Q. Wu, Y.D. Zhang, M.G. Amin, B. Himed, High-resolution passive SAR imaging exploiting structured Bayesian compressive sensing. IEEE J. Sel. Topics Sign. Process. **9**(8), 1484–1497 (2015)

19. T. AbdallaA bdi, T. Alkhodary Mohammad, A. Alawsh Saleh, Muqaibel: through-the-wall radar imaging exploiting Pythagorean apertures with sparse reconstruction. Digit. Sig. Process. A Rev. J. **61**, 86–96 (2017)

20. S. Li, W. Chen, W. Liu, J. Yang, X. Ma, Fast 2d super resolution ISAR imaging method under low signal-to-noise ratio. IET Radar, Sonar Navig. **11**(10), 1495–1504 (2017)

21. H. Nikaein, A. Sheikhi, S. Gazor, Target detection in passive radar sensors using least angle regression. IEEE J. Sel. **21**(4), 4533–4542 (2021)

22. W. Feng, J.-M. Friedt, G. Cherniak, M. Sato, Batch compressive sensing for passive radar range-doppler map generation. IEEE Trans. Aerosp. Electron. Syst. **55**(6), 3090–3102 (2019)

23. J. Wen, J. Yi, X. Wan, Sparse representation for target parameter estimation in CDR-based passive radar. IEEE Geosci. Remote. Sens. Lett. **18**(6), 1024–1028 (2021)

24. G. Leibovitz, R. Giryes, Efficient least residual greedy algorithms for sparse recovery. IEEE Trans. Signal Process. **68**, 3707–3722 (2020)

25. P. Gong, Z. Shao, G. Tu, Q. Chen, Transmit beampattern design based on convex optimization for MIMO radar systems. Sign. Processing. **94**, 195–201 (2014)

26. S. Khanna, C.R. Murthy, Decentralized joint-sparse signal recovery: a sparse Bayesian learning approach. IEEE Trans. Sign. Inf. Process. **3**(1), 29–45 (2017)

27. J. Wen, Z. Zhou, D. Li, X. Tang, A novel sufficient condition for generalized orthogonal matching pursuit. IEEE Commun. Lett. **21**(4), 805–808 (2017)

28. A. Kulkarni, T. Mohsenin, Low overhead architectures for OMP compressive sensing reconstruction algorithm. IEEE Trans. Circuits Syst I Regul. Pap. **64**(6), 1468–1480 (2017)

29. X. Wan, J. Wang, S. Hong, H. Tang, Reconstruction of reference signal for DTMB-based passive radar systems. in *Proceedings of IEEE CIE International Conference on Radar* (Chengdu, China, 2016) pp. 65–168

30. G. Lellouch, A.K. Mishra, M. Inggs, Design of OFDM radar pulses using genetic algorithm based techniques. IEEE Trans. Aerosp. Electron. Syst. **52**(4), 1953–1966 (2015)

31. M. Elad, (ed.): *Sparse and Redundant Representations: From Theory to Applications in Signal and Image Processing* (Springer, New York, 2010)

32. X. Wan, Z. Zhao, D. Zhang, Q. Shan, HF passive bistatic radar based on DRM illuminators. in *Proceedings of IEEE CIE International Conference on Radar* (2016), pp. 157–160